

pubs.acs.org/JPCA Article

Microwave and Computational Study of Methanesulfonic Acid and Its Complex with Water

Anna K. Huff, Nathan Love, and Kenneth R. Leopold*



Cite This: https://doi.org/10.1021/acs.jpca.3c01395



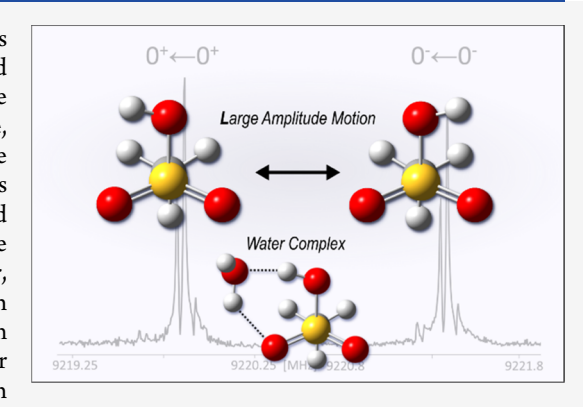
ACCESS

III Metrics & More

Article Recommendations

s Supporting Information

ABSTRACT: Spectra of methanesulfonic acid (CH₃SO₃H, MSA) and its complex with water have been studied by microwave spectroscopy and density functional theory calculations. For the monomer, spectra were obtained for both the parent and $-\mathrm{OD}$ isotopologues and, in each case, revealed a pair of tunneling states that are attributed to large amplitude motion of the hydroxyl hydrogen about the S $-\mathrm{O}(\mathrm{H})$ bond. Transitions crossing between tunneling states were not found in the parent spectrum and are estimated to be outside the range of the spectrometer, thus precluding the direct determination of the tunneling energy. For the $-\mathrm{OD}$ form, however, the tunneling energy was determined to be $\Delta E = 6471.9274(18)$ MHz from direct measurement of the cross-state c-type transitions. In its complex with water, the acidic hydrogen of the MSA forms a hydrogen bond with the water oxygen. A secondary hydrogen bond involving the water hydrogen and an



 SO_3 oxygen completes a six-membered ring, forming a cyclic structure typical of hydrated oxyacids. No evidence of internal motion was observed. Rotational spectra of the $CH_3SO_3H\cdots D_2O$ and $CH_3SO_3D\cdots D_2O$ isotopologues were also obtained and analyzed. Comparison with theoretical calculations confirms the cyclic structure, though the orientation of the unbound water hydrogen is ambiguous.

■ INTRODUCTION

The role of methanesulfonic acid (CH₃SO₃H, MSA) in the atmosphere has been a subject of continued interest because it is one of the stable products resulting from the oxidation of dimethyl sulfide emitted from oceans. ^{1–5} Consequently, MSA (or CH₃SO₃[–]) is a common component found in marine aerosols ^{6–9} and also has a measurable concentration in the gas phase. ^{10,11} Recently, experimental and theoretical studies have examined the potential of MSA to not only enhance growth of pre-existing mixed clusters of sulfuric acid, amines, and H₂O but also initiate new particle formation as well. ^{12–17}

MSA has been characterized by many spectroscopic techniques. Vibrational spectra have been reported for the monomer in the liquid and vapor phases, ^{18–21} at the air—water interface, ^{22,23} and in an argon matrix for both the monomer and its water complex. ²⁴ Cavity ring-down spectroscopy has also been used to record the vapor-phase —OH overtone spectrum of the free acid. ²⁵

Fundamental interest in MSA stems from its similarity to the superacid, triflic acid (CF₃SO₃H). Microwave spectra of triflic acid and its -OD isotopologue have been reported²⁶ and reveal a tunneling motion arising from the wagging of the -OH(D) moiety between two equivalent minima on either side of a C_s symmetric transition state. The hydrates of triflic acid, CF₃SO₃H···(H₂O)_{n=1-3},²⁷ as well as its complex with trimethylamine,²⁸ have also been investigated by microwave techniques. These studies have shown that triflic acid

undergoes proton transfer when complexed with only one trimethylamine molecule but requires three water molecules to realize proton transfer in a cold molecular complex. MSA, though still a strong acid with a pK_a of -1.9, is weaker than triflic acid, whose pK_a is -5.90. Thus, a comparison of triflic acid with MSA provides an opportunity to explore the differences in both the internal dynamics and the propensity for proton transfer that arise from the replacement of the electron-withdrawing CF_3 with the electron-donating CH_3 .

In this work, we report the microwave spectra of MSA and its complex with one water molecule. In addition to the parent species, spectra are also reported for the CH_3SO_3D , $CH_3SO_3H\cdots D_2O$, and $CH_3SO_3D\cdots D_2O$ isotopologues. The experimental work is supplemented by computations that help to elucidate the tunneling path and barrier for hydroxyl torsion in the monomer, as well as to aid in the structural interpretation of the observed spectra of the monohydrate.

Received: February 28, 2023 Revised: March 30, 2023



COMPUTATIONAL METHODS

Methanesulfonic Acid Monomer. The minimum energy structure of methanesulfonic acid was optimized at the M06-2X/6-311++G(3df,3pd) level of theory using the Gaussian16 suite of programs. The resulting structure is shown in Figure 1. The hydroxyl group is closely aligned with the S1=O6

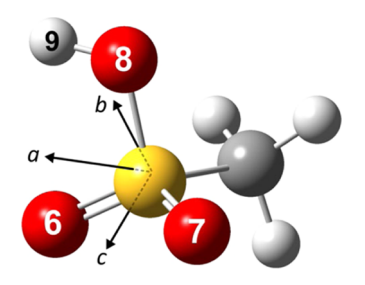


Figure 1. Computed structure of methanesulfonic acid in its minimum energy configuration calculated at the M06-2X/6-311++G(3df,3pd) level of theory. The a-, b-, and c-axes are the principal axes of the inertial tensor of the parent isotopologue.

bond, with a O6–S–O8–H9 dihedral angle of only 4.5°. An equivalent minimum energy geometry is found when the –OH is instead aligned with the S1=O7 bond. Predicted spectroscopic constants and dipole moment components are given in Table 1. Cartesian coordinates for this and all calculated structures reported in this work are given in the Supporting Information.

Table 1. Theoretical Constants for Methanesulfonic Acid^a

	CH ₃ SO ₃ H	CH ₃ SO ₃ D
A [MHz]	4940.1	4851.0
B [MHz]	4607.9	4505.1
C [MHz]	4516.5	4363.6
$ \mu_{ m a} $ [D]	2.0	1.1
$ \mu_{b} $ [D]	3.1	3.7
$ \mu_{\rm c} $ [D]	1.1	0.4
χ_{aa} [MHz]		0.0708
$\chi_{bb} - \chi_{cc} [\mathrm{MHz}]$		-0.0750

^aObtained from M06-2X/6-311++G(3df,3pd) calculations.

A scan of the potential energy along the C-S-O-H dihedral angle is shown in Figure 2 where it can be seen that two distinct barriers separate the equivalent potential energy minima. Two C_s symmetric transition-state structures (both with $\mu_c = 0$ D) were located, one in which the O–H is oriented in a syn configuration relative to the S-C bond (0/360°) and one in an anti configuration (180°). The transition-state structure with the -OH in the syn orientation was calculated to be 6.27 kcal mol⁻¹ (5.87 kcal mol⁻¹ with zero-point energy (ZPE) corrections) above the minimum energy structure, while that with the -OH oriented anti was only 0.69 kcal mol^{-1} (0.33 kcal mol^{-1} with ZPE corrections) above the minimum. The latter is virtually identical to the 0.71 kcal mol⁻¹ barrier calculated by Lane et al. at the B3LYP/aug-ccpV(T+d)Z level of theory.²⁵ Additionally, a transition state corresponding to the internal rotation of the methyl group was located after imposing a 60° rotation of the CH₃ from its minimum energy orientation and optimizing the resulting structure to a transition state. The optimized energy in this case was 2.73 kcal mol⁻¹ (955 cm⁻¹) above that of the

minimum energy structure and this value is taken to be the predicted V_3 internal rotation barrier of the methyl group.

Methanesulfonic Acid-Water. Extensive theoretical work on hydrated clusters containing methanesulfonic acid has been previously presented. $^{12,24,31-35}$ The two lowestenergy structures of the monohydrate have been recalculated here to obtain information directly relevant to rotational spectroscopy, though we note that the structural and energetic results are generally in good agreement with the literature. As above, calculations were performed at the M06-2X/6-311+ +G(3df,3pd) level of theory and the results are shown in Figure 3. The lowest-lying structures display the typical³⁶ formation of a hydrogen-bonded ring, with a primary hydrogen bond formed between the -OH hydrogen of MSA and water oxygen, and a secondary hydrogen bond formed between a water hydrogen and a S=O oxygen. As may be seen in the figure, the two structures are very similar, differing mainly in the orientation of the unbound H₂O hydrogen. In structure A, the unbound hydrogen is oriented away from CH3, while in structure B it is tilted toward CH3. Structure A is the lowerenergy form by 0.68 kcal mol⁻¹ (0.61 kcal mol⁻¹ with ZPE corrections) and is also consistently predicted to be the global minimum energy structure from other levels of theory reported in previous works noted above. At the level of theory employed here, structure A lies 13.8 kcal mol⁻¹ (11.4 kcal mol⁻¹ with ZPE corrections) below the sum of the free monomer energies while structure B is only 13.1 kcal mol⁻¹ lower in energy (10.8 kcal mol⁻¹ with ZPE corrections). The barrier to methyl group internal rotation was calculated for both conformers as described above for the monomer, with values of $V_3 = 1000$ and 984 cm⁻¹ predicted for A and B, respectively. The relative energies of the two conformers and their predicted spectroscopic constants are summarized in Table 2.

Although the two conformers of the water complex differ in energy by almost 0.7 kcal mol⁻¹, the hydrogen-bonded rings themselves are very similar, consistent with previous calculations. Using the atom numbering in Figure 3, the hydrogen-bond interactions in the primary O8–H9···O10 hydrogen bond are almost identical, with values of 1.661 and 1.656 Å for structures A and B, respectively. Likewise, for the secondary hydrogen bond (O6···H12–O10), the interaction distances are 2.013 and 2.027 Å. Slight differences in angles accompany the change in conformation, but the two ring structures are, for all practical purposes, the same.

EXPERIMENTAL SECTION

Spectra of the MSA monomer were recorded in an initial series of experiments, and spectra of the MSA-H₂O complex were subsequently obtained after adding water to the expansion and applying some minor adjustments of experimental conditions. Spectra were taken using a tandem cavity and chirped-pulse Fourier transform microwave spectrometer, details of which have been described previously. 37,38 For both the monomer and the complex, a small sample (~2 mL) of liquid methanesulfonic acid (Sigma-Aldrich, 99.5%) was heated to 90-100 °C in a stainless steel reservoir to produce sufficient vapor pressure to observe signal in the broadband spectrum. The reservoir was located only a few inches upstream of the nozzle in order to reduce the amount of gas line needed to be heated and passivated. A continuous stream of 0.5 atm argon was flowed over the liquid to entrain the vapor, whereupon it was injected into a supersonic argon expansion about 5 mm downstream from the nozzle orifice. The injection was

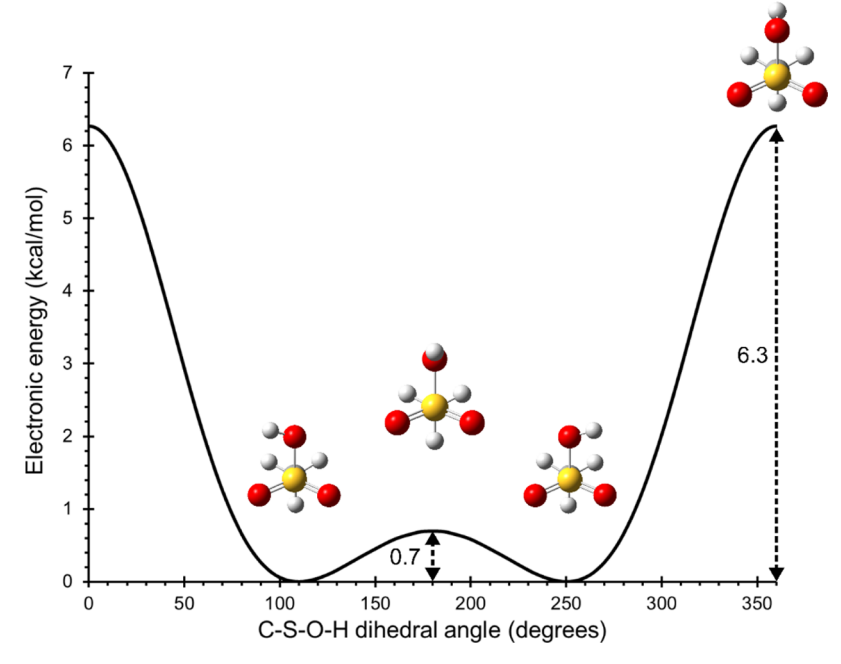


Figure 2. Potential energy scan of the methanesulfonic acid C–S–O–H dihedral angle in 2° increments from M06-2X/6-311++G(3df,3pd) calculations. The smallest barrier is 0.7 kcal mol⁻¹ and occurs when the hydroxyl hydrogen is oriented *anti* (180°) with respect to the S–C bond. When the hydroxyl hydrogen is oriented *syn* (0/360°) with respect to the S–C bond, the barrier is 6.3 kcal mol⁻¹. Equivalent structures lie at the potential minima at 110 and 250°.

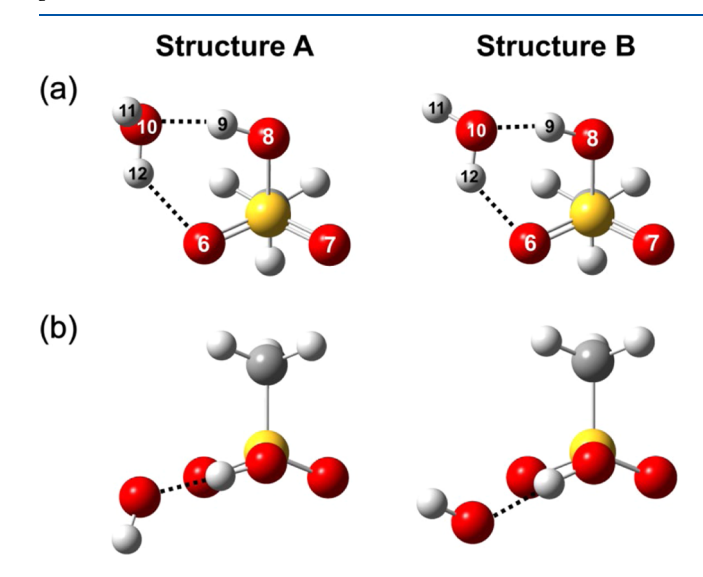


Figure 3. Two lowest-lying minimum energy structures of $CH_3SO_3H\cdots H_2O$ from M06-2X/6-311++G(3df,3pd) calculations shown from (a) the front and (b) the top view of the complexes. Structure A is predicted to be the global minimum, lying 0.68 kcal mol^{-1} (0.61 kcal mol^{-1} with zero-point corrections) lower in energy than structure B.

accomplished through a 0.020 in. inner diameter hypodermic needle, as described previously. It was found necessary to use a hypodermic needle made from 316 stainless steel (rather than 304 stainless steel) to reduce corrosion and clogging. The expansion itself was created by pulsing argon through the 0.8 mm orifice of a stainless steel cone nozzle at a stagnation pressure of 1 atm. Spectra for CH_3SO_3D were observed by passing 1 atm argon through liquid D_2O (Cambridge Isotope Laboratories, 99.9%) and creating CH_3SO_3D in situ from on-

Table 2. Theoretical Constants of the Two Lowest-Energy Conformers of CH₃SO₃H-H₂O^{a,b}

	$CH_3SO_3H\cdots H_2O$	
	A	В
A [MHz]	4683.2	4725.8
B [MHz]	1896.1	1872.0
C [MHz]	1850.3	1833.9
$ \mu_{ m a} $ [D]	2.2	1.7
$ \mu_{ m b} $ [D]	2.3	4.7
$ \mu_{ m c} $ [D]	0.3	0.02
$V_3 \left[\mathrm{cm}^{-1} \right]^c$	1000	984
rel. energy [kcal mol ⁻¹]	-13.8	-13.1
rel. energy + ZPE [kcal mol ⁻¹]	-11.4	-10.8

^aCalculated at the M06-2X/6-311++G(3df,3pd) level of theory. Complex energies are relative to the sum of the free monomer energies. ZPE stands for zero-point energy. ^bThe predicted equilibrium structures are shown in Figure 3. ^cMethyl group internal rotation barrier.

the-fly H/D exchange between the CH_3SO_3H/D_2O vapors in the supersonic jet.

For CH₃SO₃H···H₂O spectra, MSA was introduced under the same conditions as described above for the monomer except that a hypodermic needle with a 0.016 in. inner diameter was found to optimize the signal of the complex (instead of the 0.020 in. inner diameter needle used for the monomer studies). H₂O was introduced in the expansion by bubbling argon through a reservoir of liquid water at a stagnation pressure of about 1.3 atm and pulsing the Ar/H₂O gas mixture through the same nozzle described above. Spectra for CH₃SO₃H···D₂O and CH₃SO₃D···D₂O were collected by seeding the argon with D₂O instead of H₂O. Observed transition frequencies and assignments for both the monomer and the monohydrate are provided in the Supporting Information.

RESULTS

Methanesulfonic Acid Monomer. Chirped-pulse spectra of MSA in argon were collected in 3 GHz segments between 6 and 18 GHz, with free-induction decay (FID) signals recorded for 20 μ s. Each 3 GHz segment was the result of averaging between 100,000 and 500,000 FIDs. Higher frequencies in the 18.4-21.4 GHz frequency range were also accessed using the upper sideband mixing of the 3 GHz sweep with 18.2 GHz (where the lower sideband mixing of the broadband sweep is used to generate the 15-18 GHz spectrum). The simulated semirigid rotor spectrum using the theoretical rotational constants and dipole moment components (Table 1) shows that a-, b-, and c-type transitions from only J'' = 0 and 1 are expected within the range of the broadband spectrometer and indeed, only three strong lines were initially found. Three more strong lines, however, were located at about 18.2 GHz using the cavity spectrometer. Moreover, upon further scanning, another set of much weaker transitions was located, each in the vicinity of one of the observed stronger transitions. These appeared within 0.3-6.9 MHz above or below their stronger counterpart and had about one tenth the intensity. Eventually, all 18 observed transitions were measured on the cavity spectrometer and their frequencies are listed in Table 3.

Table 3. Observed Microwave Frequencies (in MHz) and Rotational Assignments of CH₃SO₃H^a

	strong (0+)	weak (0 ⁻)
$1_{01} \leftarrow 0_{00}$	9106.253	9105.496
$1_{10} \leftarrow 0_{00}$	9462.703	9465.062
$2_{02} \leftarrow 1_{10}$	17,855.759	17,851.605
$2_{12} \leftarrow 1_{11}$	18,210.443	18,205.945
$2_{02} \leftarrow 1_{01}$	18,212.209	18,211.172
$2_{11} \leftarrow 1_{10}$	18,213.467	18,217.033
$2_{11} \leftarrow 1_{01}$	18,569.916	18,576.602
$2_{20} \leftarrow 1_{10}$	19,278.553	19,278.873
$2_{21} \leftarrow 1_{11}$	19,279.772	19,284.645

"Lines at 18.2 GHz were only observed on the cavity instrument due to the accessible frequency range. Lines at or above 18.5 GHz were first seen on the chirped-pulse spectrometer and later remeasured on the cavity system.

Uncertainties of these measurements were only 1–3 kHz for most transitions but were up to 10 kHz for some lines near 19.3 GHz due to background noise in the cavity modes in this spectral region.

The discovery of the second set of (weaker) transitions indicates the presence of a pair of tunneling states (denoted 0⁺ and 0⁻). As in previous work on triflic acid, ²⁶ these states are reasonably ascribed to hydroxyl torsion about the S-O(H) bond (i.e., tunneling between the two potential minima in Figure 2). Aided by closed loops, the best fits were obtained by assigning only a- and c-type transitions within individual tunneling states (i.e., $0^+ \leftarrow 0^+$ and $0^- \leftarrow 0^-$), with the groundand excited-state transitions assigned to the strong and weak set of lines, respectively. For the parent, the correspondence between the strong set of transitions and the ground state is based on anticipated Boltzmann populations associated with the large tunneling splitting, discussed below. For the -OD isotopologue, the same argument applies and is strongly supported by the positive value of $\Delta E = E(0^{-}) - E(0^{+})$ obtained when the stronger set of lines is assigned to the ground state.

A surprising feature of the spectra is that the c-type transitions within each tunneling state were assigned to lines that were at least two to three times stronger than the observed a-type transitions, which initially seemed inconsistent with the predicted magnitudes of the dipole moment components along the *a*- and *c*-axes ($|\mu_a|$ = 2.0 D, $|\mu_c|$ = 1.1 D). Indeed, the *c*-type lines had initially been assigned as b-type transitions because the largest predicted dipole component is along the *b*-axis ($|\mu_b|$ = 3.1 D). However, attempts to fit the spectra with those assignments resulted in negative values of (B - C). The observed and predicted relative intensities are shown in the broadband spectral excerpt in Figure 4a,c. Figure 4b shows a simulated spectrum with swapped theoretical values of μ_b and μ_{o} and clearly demonstrates a better reproduction of the observed intensities. The origin of this apparent axis switching is discussed in a later section.

The two states were initially fit separately to a semirigid rotor Watson A-reduced Hamiltonian in the I representation using Pickett's SPFIT program. The results are shown in Table 4. Even with small line sets containing only nine frequencies involving only J'' = 0 and 1, the resulting RMS values for the 0^+ and 0^- states are seen to be 152 and 129 kHz, respectively, i.e., much higher than experimental uncertainty. Interestingly, the values of (B - C) from these fits are only about 1.5 and 4.5 MHz for the 0^+ and 0^- states, respectively, which are quite different than the computationally predicted value 91 MHz.

No b-type lines at the locations predicted from the above fits could be found during spectral searches on the cavity spectrometer and no additional lines were observed in the broadband spectrum. The assignment of a- and c-type lines to intrastate transitions indicates that μ_a and μ_c retain the same sign upon hydroxyl tunneling between the two potential minima. This leaves the b-type transitions to be the cross-state transitions $(0^+ \leftarrow 0^- \text{ and } 0^- \leftarrow 0^+)$. In other words, it is μ_b that is inverted by the tunneling motion. Accordingly, the b-type lines are expected to be displaced from their rigid rotor positions by an amount approximately equal to the tunneling energy, $\Delta E \equiv E(0^-) - E(0^+)$. The lack of observable b-type transitions in the broadband spectrum indicates that this displacement moves them outside the operational range of the spectrometer.

The somewhat large residuals in the individual semirigid rotor fits of the 0^+ and 0^- states suggest that these states are coupled and need to be treated simultaneously. The following Hamiltonian was used for a simultaneous fit of the ground (0^+) and excited (0^-) state transitions of the parent form using Pickett's SPFIT program⁴¹

$$H = \sum_{n=0}^{1} \left[H_{\text{rot}}^{(n)} + H_{\text{cd}}^{(n)} + \delta_{n,1} \Delta E \right] + H_{\text{int}}$$
 (1)

Here, $H_{\rm rot}$ and $H_{\rm cd}$ represent the rigid rotor Hamiltonian and Watson A centrifugal distortion Hamiltonian in the $I^{\rm r}$ representation, respectively. The 0^+ and 0^- states are represented by n=0 and 1, respectively, and $\delta_{n,1}$ is the Kronecker delta. Each state has its own set of vibrationally averaged rotational constants, and the correct set is used in the sum when creating the matrix representation of H. $H_{\rm int}$ is the interaction Hamiltonian coupling the tunneling states, 42 given by

$$H_{\text{int}} = F_{bc}(P_b P_c + P_c P_b) + F_{ab}(P_b P_a + P_a P_b)$$
 (2)

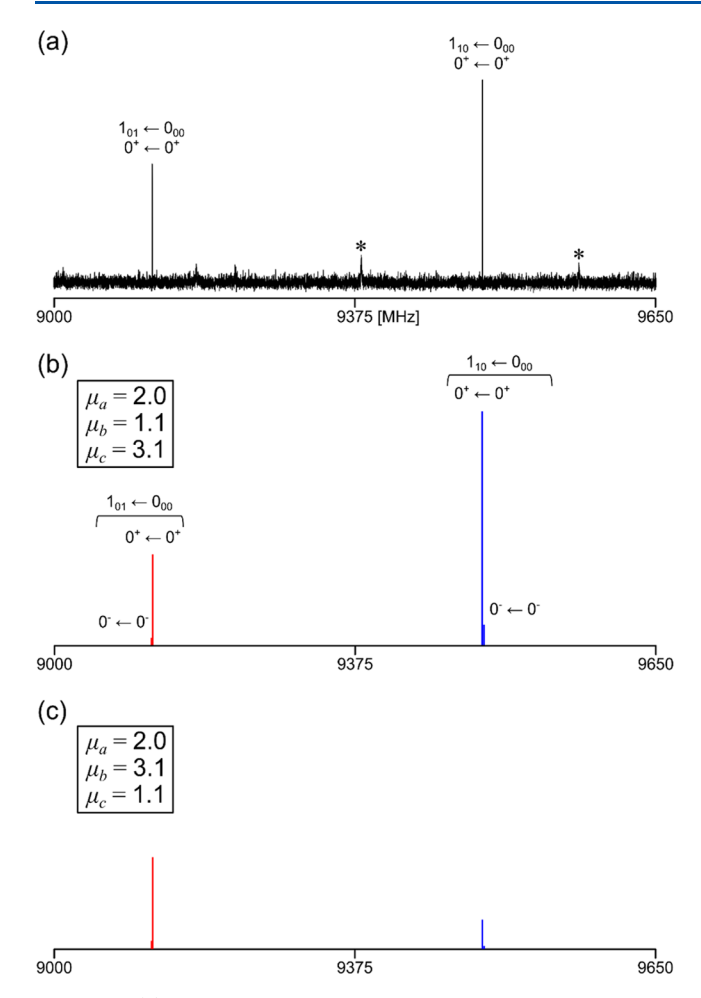


Figure 4. (a) Excerpt of the chirped-pulse broadband spectrum of MSA and argon between 9000 and 9650 MHz. The assigned groundstate partners of the $1_{01} \leftarrow 0_{00}$ and $1_{10} \leftarrow 0_{00}$ transitions are labeled. The excited-state partners of these transitions were located only 0.7 and 2.4 MHz below and above their ground-state counterparts in the cavity spectra, respectively, but did not have sufficient S/N to be observed in the broadband spectrum. The features labeled with an asterisk (*) are known instrumental artifacts. (b) Simulated spectrum at 3 K using fitted constants from the combined two-state fit with ΔE = 150 GHz. The dipole moment components are the same as the theoretical values except the values of μ_b and μ_c have been swapped. The b-type transition is displaced by the tunneling energy. The excited-state $(0^- \leftarrow 0^-)$ transitions for the $1_{01} \leftarrow 0_{00}$ and $1_{10} \leftarrow 0_{00}$ transitions were measured from cavity spectra and are 0.757 MHz below and 2.359 MHz above their ground-state counterparts, respectively. (c) Simulated spectrum at 3 K using the same fitted constants as described for panel (b), but here using the dipole moment components from the M06-2X/6-311++G(3df,3pd) level of theory. The vertical scale is the same as on panel (b), but the relative intensities of the transitions differ due to the switching of $\mu_{\rm b}$ and $\mu_{\rm c}$.

For CH₃SO₃H, both the F_{bc} and F_{ab} coupling terms are allowed by symmetry. Only a single Δ_J parameter common to both states was used and, interestingly, is determined to be close to the average of the values obtained in the separate fits.

Because of the absence of cross-state transitions in the data set, the value of the tunneling energy cannot be determined from the spectrum. Nevertheless, the constraint of ΔE to a reasonable value allows the interaction constants $|F_{bc}|$ and $|F_{ab}|$ to be incorporated. The constants obtained by fixing ΔE at 150 GHz are listed in Table 4 under "combined fit". This choice was made based on the estimate by Lane et al. of 5 cm⁻¹

calculated using a one-dimensional, semiclassical approximation. We note, however, that a range of fixed values from 20 to 250 GHz was tried in order to test the sensitivity of the fit. As expected, the interaction constants varied depending on the value of ΔE chosen, but the fitted rotational constants and RMS residual remained unchanged. Moreover, although the coupling constants themselves depended on the fixed value of ΔE chosen, the ratio $(F_{bc}^2 + F_{ab}^2)/\Delta E$ remained the same. As seen in Table 4, with the inclusion of the interaction terms, the RMS residual decreased from 120–152 kHz to about 6 kHz. Note that fitting the coupling terms individually with a fixed ΔE resulted in a nonconverged fit in the case of F_{bc} (and its value was not determined). For F_{ab} , the value was determined to be 69.2(14) MHz when ΔE was fixed to 150 GHz, but the RMS residual (90 kHz) was significantly larger than the 6 kHz value obtained in the fit employing both coupling constants.

A pair of states was also observed for CH₃SO₃D in the broadband spectra, and the deuterium hyperfine structure was resolvable in the cavity spectra for most transitions. The hyperfine patterns were consistent for the ground- and excited-state partners of any particular rotational transition, as seen in the cavity spectra in Figure 5, and were used as an early aid in matching and assigning tunneling state pairs.

In contrast to the assignments discussed above for the parent species, *a-*, *b-*, and *c-*type transitions were all observed and successful fits were achieved only when *a-* and *b-*type lines were assigned as intrastate transitions while *c-*type transitions were assigned as cross-state transitions. This reversal relative to the parent exactly parallels that observed for triflic acid. Additionally, although the excited-state transitions appeared at somewhat lower intensities than their ground-state counterparts, unlike for the parent species they were generally comparable in strength and, indeed, were often more than half the signal intensity of the ground-state transitions.

In total, 103 hyperfine components were measured between 2.7 and 19.7 GHz and assigned to 31 rotational transitions consisting of 25 R-branch and 6 Q-branch transitions. The Rbranch lines ranged from J'' = 0 to J'' = 2 with transitions involving up to $K_a'' = 1$, and Q-branch transitions were all ctype and ranged from J = 1 to J = 4 involving up to $K_a'' = 1$. The separation of the ground- and excited-state partners of the a- and b-type transitions was as little as 1.5-4 MHz for the J'' = 0 lines and between 23 and 47 MHz for J'' = 1 lines. The higher-frequency partner $(0^- \leftarrow 0^+)$ of the *c*-type $1_{10} \leftarrow 0_{00}$ transition was located about 6.4 GHz above its rigid rotor position, which is approximately the value of ΔE . The frequencies were fit to a Hamiltonian similar to that in eq 1 with the addition of an $H_{\rm O}$ term for the deuterium quadrupole coupling interaction. However, because the c-type transitions were observed to cross tunneling states, the symmetry rules change compared to the parent such that the F_{bc} and F_{ac} coupling terms are allowed. Thus, H_{int} becomes the expression given below in eq 3.

$$H_{\text{int}} = F_{bc}(P_b P_c + P_c P_b) + F_{ac}(P_a P_c + P_c P_a)$$
 (3)

The constants obtained from a combined two-state fit are given in Table 5, where it may be seen that in this case, independent values of Δ_I for the two states were used.

Methanesulfonic Acid–Water. After averaging approximately 200,000 FIDs (each collected for 20 μ s), only a few lines that were dependent on both MSA and H₂O were found in the broadband spectrum. Guided by the predicted constants and dipole moment components for both conformers given in

Table 4. Spectroscopic Constants of CH₃SO₃H^a

	separate fits		combi	ned fit
	0+	0-	0+	0-
A [MHz]	4908.810(76)	4909.527(77)	4908.8437(15)	4909.5223(17)
B [MHz]	4553.939(66)	4555.478(61)	4553.8856(12)	4555.5220(12)
C [MHz]	4552.443(60)	4549.925(60)	4552.4166(11)	4549.9351(13)
Δ_I [kHz]	21.9(70)	-18.6(67)	1.20	(10)
$ F_{bc} [MHz]^b$			58.43	3(31)
$ F_{ab} [MHz]^b$			80.33	2(17)
$\Delta E [MHz]$			[150	0000]
N^c	9	9	1	8
RMS $[kHz]^d$	152	129	5	.8

^aNumbers in parentheses are one standard error in the least-squares fit. ^bSign cannot be determined in the fit and the value is highly dependent on the chosen fixed value of ΔE . For this fit, ΔE was fixed to 150.0 GHz. See text for discussion. ^cNumber of transitions included in the fit. ^dRoot-mean-square deviation of the value of the observed frequencies minus the calculated frequencies from the least-squares fit.

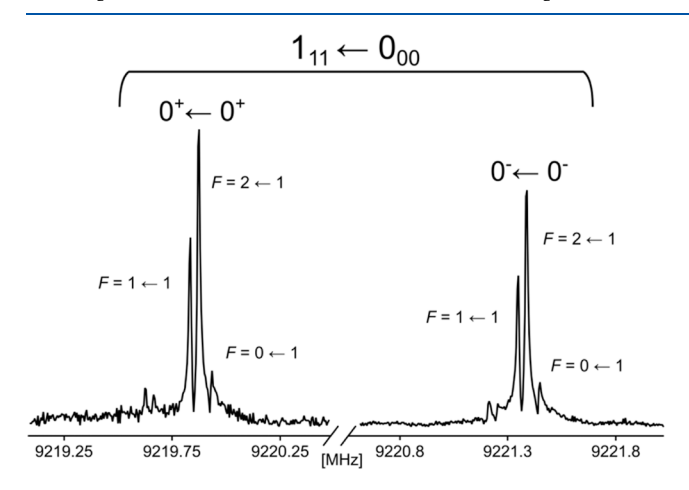


Figure 5. Cavity spectra of the CH₃SO₃D ground- $(0^+ \leftarrow 0^+, \text{left})$ and excited $(0^- \leftarrow 0^-, \text{right})$ -state b-type $1_{11} \leftarrow 0_{00}$ transition resulting from the average of 1000 and 4000 FID signals, respectively, where each FID was collected for 140.8 μ s. The F = J + I quantum number assignments for the deuterium hyperfine components are also shown, where the nuclear spin of deuterium is I = 1. The small features to the left of the 9219.75 and 9221.3 MHz cavity frequencies are instrumental artifacts.

Table 5. Spectroscopic Constants of CH₃SO₃D^a

	CH ₃ SO ₃ D		
	0+	0-	
A [MHz]	4803.80808(71)	4803.78759(78)	
B [MHz]	4454.61687(90)	4454.34170(64)	
C [MHz]	4416.67483(73)	4416.97431(80)	
$\Delta_{J} [\mathrm{kHz}]$	1.244(88)	1.508(85)	
$ F_{bc} [MHz]^b$	63.243	39(69)	
$ F_{ac} [MHz]^b$	104.4014(61)		
$\Delta E [\mathrm{MHz}]$	6471.9274(18)		
χ_{aa} [MHz]	-0.0339(30)	-0.0443(30)	
$(\chi_{bb}-\chi_{cc})$ [MHz]	-0.3028(64)	-0.2976(44)	
N^c	103		
RMS $[kHz]^d$	4.2		

"Numbers in parentheses are one standard error in the least-squares fit. "Sign cannot be determined in the fit. "Number of deuterium hyperfine components included in the fit. The 103 hyperfine components were assigned to 31 rotational transitions. "Root-mean-square deviation of the value of the observed frequencies minus the calculated frequencies from the least-squares fit.

Table 2, both a- and b-type transitions were then located and measured from cavity spectra with uncertainties of less than 3 kHz. Once a successful fit was obtained, attempts were made to locate c-type transitions on the cavity spectrometer. However, none were observed even after significant spectral averaging, likely due to the small predicted values of μ_c ($|\mu_c| = 0.3$ and ~ 0.0 D for conformers A and B, respectively). In total, 31 lines were found and assigned to 16 a-type transitions and 15 b-type transitions (including 12 R-branch and 3 Q-branch transitions) ranging from J'' = 0 to J'' = 5 and up to $K_a'' = 3$. Although the significant dependence of cavity tuning across different frequencies makes the direct comparison of transition intensities difficult, the a- and b-type transitions appeared in the spectra with approximately similar intensities.

For both deuterated isotopologues, CH₃SO₃H···D₂O and CH₃SO₃D···D₂O₄ 17 lines were measured and included 13 atype and 4 b-type transitions. For $CH_3SO_3H\cdots D_2O_7$, rotational transitions ranged from J'' = 1 to J'' = 3 and included up to $K_a^{"}$ = 2. A similar set of transitions was obtained for CH₃SO₃D···· D_2O except the J range increased up to J''=4. Hyperfine structure from the deuterium nuclei was too congested to assign in almost all observed transitions and resulted in slightly higher measurement uncertainties relative to the parent spectra (3-6 kHz). Likely due to isotopic scrambling of CH₃SO₃H with D_2O , the intensities of the isotopologue transitions were generally low. The observed frequencies for all species were fit to a semirigid rotor Watson A-reduced Hamiltonian using Pickett's SPFIT program and the resulting spectroscopic constants are given in Table 6. No additional lines were observed for either A/E methyl internal rotor state pairs or spectral pairs from internal H₂O motion.

DISCUSSION

Methanesulfonic Acid Monomer. The observed and predicted spectroscopic constants of MSA as well as the isotope shifts in the rotational constants are compared in Table 7. It can be seen that the calculated rotational constants for the parent form are between 0.6 and 1.2% of the observed values. The deuterium isotope shifts in the rotational constants are somewhat worse, with agreement in the 3–15% range. Given the presence of large amplitude –OH wagging, this may not be too surprising. Overall, however, the agreement between the observed and calculated rotational constants is quite reasonable and leaves no doubt as to the identity of the observed species. Interestingly, the calculated value of *B* is too large while that of *C* is too small, resulting in a predicted

Table 6. Spectroscopic Constants of Observed Methanesulfonic Acid Monohydrate Isotopologues^a

	$CH_3SO_3H\cdots H_2O$	$CH_3SO_3H\cdots D_2O$	$CH_3SO_3D\cdots D_2O$
A [MHz]	4673.1751(25)	4633.9789(23)	4593.2712(49)
B [MHz]	1856.51551(64)	1745.60897(30)	1730.8673(10)
C [MHz]	1812.55884(66)	1708.69423(40)	1698.9973(10)
Δ_{J} [kHz]	0.7160(82)	0.6400(97)	0.624(22)
Δ_{JK} [kHz]	17.052(43)	15.817(50)	15.01(16)
$\Delta_K [\mathrm{kHz}]$	-15.66(64)		
$\delta_{J} [\mathrm{kHz}]$	0.0572(94)		
N^b	31	17	17
RMS $[kHz]^c$	3.8	2.6	6.1

"Numbers in parentheses are one standard error in the least-squares fit. "Number of transitions included in the fit. "Root-mean-square deviation of the value of the observed frequencies minus the calculated frequencies from the least-squares fit.

(B-C) which is much greater than the observed value (91.4 vs 1.469 MHz). This small actual value of (B-C) has significance with regard to the switching of the b- and c-inertial axes, as discussed below. In addition, we note a departure between the observed and theoretical deuterium quadrupole coupling constants, where the observed χ_{aa} is -0.0339(30) MHz compared to a positive value of 0.0708 MHz from theory. Somewhat similarly, the observed value of $(\chi_{bb}-\chi_{cc})$ is a more negative value of -0.3028(64) MHz than the predicted value of -0.075 MHz. The absolute magnitudes of these discrepancies likely reflect the difficulty associated with calculating a near-zero value and may be compounded by the large amplitude wagging of the $-\mathrm{OD}$ moiety in the vibrationally averaged structure.

An unusual feature of this system is that b-type transitions cross between tunneling states for the $-\mathrm{OH}$ species but c-type transitions cross in the $-\mathrm{OD}$ spectrum. This is exactly analogous to the situation previously observed and discussed at length for triflic acid. Briefly, as for triflic acid, the predicted C_s transition states for both isotopologues are symmetric in the ab-plane ($\mu_c = 0$), suggesting c-type transitions would cross between the states in both cases (since the c-component of the dipole moment would invert upon hydroxyl torsion). However, without the $-\mathrm{OH}$ hydrogen, the system is a symmetric top, with no unique orientation of the b- and c-axes. The presence of the hydrogen breaks symmetry, but the system is still sufficiently close to symmetric that small changes in the structure can switch the definition of the axes. Specifically for MSA, if the S-O bond in the

theoretical transition-state structure is decreased by only 0.04 Å from 1.59 to 1.55 Å, the –OH form switches to become symmetric in the ac-plane ($\mu_{\rm b}=0$) while the –OD form stays symmetric in the ab-plane ($\mu_{\rm c}=0$). The same result can also be achieved when the C–S–O angle is increased by 3° (from 97.3 to 100.3°) while the angles of the C–S=O bonds are decreased by 2° (from 110.1 to 108.1°). Moreover, it is reasonable that the accumulation of even smaller deviations from the theoretical structure could lead to similar effects. This axis switching further accounts for the need to swap the values of $\mu_{\rm b}$ and $\mu_{\rm c}$ to reasonably reproduce relative intensities (Figure 4).

As noted above, the tunneling frequency for deuterated MSA has been directly determined from the observed spectra but the equivalent determination was not possible for the parent form. This is consistent with the estimate of 150 GHz by Lane et al.²⁵ which places the *b*-type transitions outside the range of the spectrometer. Alternate methods of estimating the tunneling frequency for the parent form lead to the same conclusion. Specifically, the breadth of experimental work on systems with similar -OH torsional motion has led to the development of empirical correlations between tunneling frequency and barrier height. For example, in the study of acetone cyanohydrin, 43 the authors used an apparent logarithmic relationship between ΔE and the barrier to -OH torsion to predict a value of ΔE when it also could not be determined from the microwave spectra. Using the smaller of the two predicted barrier heights for MSA of 0.69 kcal mol⁻¹ in the linear regression from ref 43 gives a value of ΔE = 224 GHz. Additionally, Medel has described various models that include correlating the tunneling energies of the -OH and -OD isotopologues of a particular species. 44 Using the observed value of the tunneling energy of CH₃SO₃D and invoking the universal correlation of ΔE for -OH and -OD species as described in ref 44 result in an estimation of $\Delta E = 64$ GHz for parent MSA. Finally, we note that, although highly dependent on assumed temperature and consistency in intensity measurements, the tunneling energy can also be estimated through Boltzmann populations. For parent MSA, testing a reasonable range of temperatures from 1.5 to 3.0 K for J'' = 0 transitions gives a rough range of $\Delta E = 62-158$ GHz. Although the range in values of these approximations is quite large, all arguments support the notion that b-type transitions that cross the tunneling doublet are displaced outside the range of the 3-18 GHz microwave spectrometer used in these studies.

Table 7. Observed and Theoretical Constants and Isotope Shifts for CH₃SO₃H and CH₃SO₃D.^a

	M06-2X/6-311++G(3df,3pd)		obse	erved ^b
	-OH	-OD	-ОН	-OD
A [MHz]	4940.1	4851.0	4908.8437(15)	4803.80808(71)
B [MHz]	4607.9	4505.1	4553.8856(12)	4454.61687(90)
C [MHz]	4516.5	4363.6	4552.4166(11)	4416.67483(73)
$\chi_{aa} \ [\mathrm{MHz}]$		0.0708		-0.0339(30)
$(\chi_{bb} - \chi_{cc})$ [MHz]		-0.0750		-0.3028(64)
$\Delta A \; [\mathrm{MHz}]$		-89.1		-105.0356(17)
$\Delta B \; [\mathrm{MHz}]$		-102.8		-99.2687(15)
$\Delta C [\mathrm{MHz}]$		-152.9		-135.7418(13)

[&]quot;Isotope shifts of the rotational constants are calculated by subtracting the parent value from that of the isotopologue. bObserved constants in the table are for the 0+ state.

Although the observation of a-, b-, and c-type spectra for the $-\mathrm{OD}$ form clearly establishes a lack of C_s symmetry, an alternate explanation for the absence of b-type transitions in the parent form involves a value of $\langle \mu_b \rangle = 0$ due to vibrational averaging of the lighter $-\mathrm{OH}$ moiety over the barrier in the double-well potential. However, while such a scenario provides a possible alternate explanation, the above arguments supporting the large tunneling splitting are strong. Searches for b-type spectra at higher frequencies could provide the spectroscopic evidence necessary to definitively distinguish between these scenarios.

Finally, it is of interest to compare MSA with triflic acid. Both exhibit a pair of tunneling states arising from hydroxyl torsion. The barriers are quite different, however, with the lower (anti) barrier in MSA of only 0.69 kcal mol⁻¹ (0.33 kcal mol⁻¹ with ZPE corrections), compared to 2.8 kcal mol⁻¹ (2.2 kcal mol⁻¹ with ZPE corrections) for triflic acid. Although the tunneling energy was not determined here for parent MSA, estimated values are orders of magnitude larger than that the 52.96784(65) MHz value determined for triflic acid. For the -OD isotopologues, the tunneling energies are again quite different, with measured values of 6471.9274(18) and 0.2460(20) MHz for MSA and triflic acid, respectively. The axis switching between the -OH and -OD forms is common to both systems, with the cross-state b-type transitions of the parent in an apparent departure from expectations based on the structure at their C_s symmetric transition state, as calculated at the M06-2X/6-311++G(3df,3pd) level of theory.

Methanesulfonic Acid-Water. Table 8 compares the observed spectroscopic constants for the MSA-H₂O complex

Table 8. Observed and Theoretical Constants of $CH_3SO_3H\cdots H_2O^{a,b}$

		M06-2X/6-311++G(3df,3pd)			
	$CH_3SO_3H\cdots H_2O$	A	% error	В	% error
A [MHz]	4673.1751(25)	4683.2	-0.2	4725.8	-1.1
B [MHz]	1856.51551(64)	1896.1	-2.1	1872.0	-0.8
C [MHz]	1812.55884(66)	1850.3	-2.1	1833.9	-1.2

[&]quot;Numbers in parentheses are one standard error in the least-squares fit. ^bPercent error is calculated as $100 \times [(observed - predicted)/observed]$.

with those obtained from the M06-2X/6-311++G(3df,3pd) calculations. The two predicted conformers are clearly very similar, differing only in the orientation of the unbound water hydrogen. Thus, while the calculated constants are sufficiently close to the observed values to confirm the overall ring structure of the system, they are not sufficiently different to identify which form was observed. (The A rotational constants match somewhat better for conformer A while the B and C constants are in better agreement for conformer B.) Similarly, as seen in Table 9, the theoretical isotopic shifts in the rotational constants for the deuterated isotopologues studied are quite similar for the two forms. Once again, the shift in the A rotational constant for both isotopologues somewhat favors structure A while the shifts in the B and C rotational constants somewhat favor structure B. However, the favorability is by a rather narrow margin and the calculated isotope shifts are generally within reason for either conformer. This, again, arises from the very similar structures of the two forms. Thus, while the rotational constants and isotope shifts confirm the identity and the overall ring structure of the complex, they do not

Table 9. Observed and Theoretical Isotope Shifts for Deuterated Species a,b

	$CH_3SO_3H\cdots D_2O$	$CH_3SO_3D\cdots D_2O$
Observed		
ΔA	-39.1962(34)	-79.9039(55)
ΔB	-110.90654(71)	-125.6482(12)
ΔC	-103.86461(77)	-113.5615(12)
Structure A		
ΔA	-40.1	-76.5
ΔB	-115.2	-130.7
ΔC	-107.7	-117.6
Structure B		
ΔA	-51.0	-87.6
ΔB	-111.2	-126.5
ΔC	-106.2	-115.9

"Isotope shifts of the rotational constants are calculated by subtracting the parent value from that of the isotopologue. "Predicted isotope shifts for structures A and B were calculated using the M06-2X/6-311++G(3df,3pd) geometries.

provide clarity as to the orientation of the nonbonded water hydrogen.

The observed relative intensities of the a- and b-type transitions provide some limited insight into the identity of the observed conformer. Referring to the predicted dipole moment components in Table 2, the relative intensities of a- and b-type spectra should be about equal for conformer A while b-type spectra are predicted to be the more intense for conformer B. Specifically, the predicted ratio of $(\mu_b/\mu_a)^2$ for conformer B is about 7.6 compared to $(\mu_b/\mu_a)^2 = 1.1$ for conformer A. As noted above, the a- and b-type spectra appeared to have similar intensities. Thus, while comparing intensities in cavity spectra can be unreliable due to the dependence on cavity mode power at different frequencies, this suggests that the observed conformer is more likely conformer A. This is consistent with the calculated relative energies of the two forms. While the measurement of c-type transitions would have more definitively shown that the observed water complex is conformer A (since $\mu_c = \sim 0.0$ for conformer B), their absence is also not entirely unexpected given the small predicted value of $|\mu_c| = 0.3 \text{ D}$.

Unsurprisingly, as for the MSA monomer, the A/E internal rotor state pairs were not resolved in the spectrum of the water complex. Indeed, the predicted V_3 barriers for the two conformers (1000 and 984 cm⁻¹ for structures A and B, respectively) were higher than that calculated for the monomer (955 cm⁻¹) and should, therefore, give rise to small separations between transitions within the A and E internal rotor states. For the observed transitions, the predicted splitting of the A/E pairs is typically less than 3 kHz and only 8–9 kHz for the a-type $K_a = 3$ transitions at J'' = 4. The disappearance of the hydroxyl torsion is expected since the water breaks the symmetry of the MSA monomer.

It is again interesting to compare the results of the MSA—water complex to the triflic acid analogue. Relative to the sum of the respective free monomer energies, the calculated binding energy of the MSA monohydrate at the global minimum energy structure ($-13.8 \text{ kcal mol}^{-1}$) is about 1.2 kcal mol⁻¹ smaller in magnitude than that of the equivalent conformer for the triflic acid analogue ($-15.0 \text{ kcal mol}^{-1}$). With ZPE corrections, the MSA—water complex is about 1.4 kcal mol⁻¹ higher in energy ($-11.4 \text{ vs} -12.8 \text{ kcal mol}^{-1}$ for the MSA—

and triflic acid—water complexes, respectively). These differences likely reflect the relative acidities of triflic acid and MSA. In this regard, it is satisfying to note that, at the M06-2X/6-311++G(3df,3pd) level of theory, the primary hydrogen bond (O9···H10) in the triflic acid monohydrate is 1.58 Å, 27 which is somewhat shorter than the 1.66 Å distance in MSA—water obtained from the calculations reported here. The two lowest-energy conformers for MSA—water and triflic acid—water are very similar, structurally. However, for triflic acid, they were effectively isoenergetic, differing in energy by only 0.05 kcal mol $^{-1}$ with ZPE corrections. Thus, in addition to affecting the binding energy and hydrogen-bond length, the replacement of CF $_3$ with CH $_3$ appears to create a preference for the orientation of the unbound hydrogen.

CONCLUSIONS

The microwave spectra of methanesulfonic acid and its water complex have been assigned. A pair of tunneling states was observed for MSA and its $-\mathrm{OD}$ isotopologue resulting from large amplitude motion of the hydroxyl group. The tunneling energy for parent MSA could not be determined, as it is likely greater than 50 GHz and outside the range of the spectrometer used in these studies. However, the tunneling energy of the $-\mathrm{OD}$ form was determined by direct measurement to be $\Delta E = 6471.9274(18)$ MHz. As in the case of the related acid, triflic acid, the b-type transitions are the cross-state transitions for parent MSA while for the $-\mathrm{OD}$ isotopologue the c-type transitions cross between tunneling states.

The two lowest-energy conformers of the MSA—water complex are predicted, each forming a six-membered ring in which the MSA acts as a hydrogen bond donor to the water oxygen. One of the water hydrogens appears to form a secondary hydrogen bond to an MSA oxygen. Calculations indicate that the two conformers differ mainly in the orientation of the unbound water hydrogen, but this orientation could not be definitively established from the spectra. The water breaks the symmetry of free MSA resulting in the disappearance of a pair of tunneling states. Methyl group internal rotation is not observed, as expected from the high calculated barrier of 1000 cm⁻¹. The monohydrates of triflic acid and MSA show structural similarities, but the energetics and primary hydrogen-bond lengths differ in a way that sensibly reflects the difference in acidity between the two acids.

ASSOCIATED CONTENT

Supporting Information

The Supporting Information is available free of charge at https://pubs.acs.org/doi/10.1021/acs.jpca.3c01395.

Tables of observed transition frequencies, assignments, and residuals from the least-squares fits, and Cartesian coordinates from calculated minimum energy and transition-state structures (PDF)

AUTHOR INFORMATION

Corresponding Author

Kenneth R. Leopold — Department of Chemistry, University of Minnesota, Minneapolis, Minnesota 55455, United States; orcid.org/0000-0003-0800-5458; Email: kleopold@umn.edu

Authors

Anna K. Huff – Department of Chemistry, University of Minnesota, Minneapolis, Minnesota 55455, United States Nathan Love – Department of Chemistry, University of Minnesota, Minneapolis, Minnesota 55455, United States

Complete contact information is available at: https://pubs.acs.org/10.1021/acs.jpca.3c01395

Notes

The authors declare no competing financial interest.

ACKNOWLEDGMENTS

This work was supported by the National Science Foundation (Grant No. CHE 1953528) and the Minnesota Supercomputing Institute.

REFERENCES

- (1) Charlson, R. J.; Lovelock, J. E.; Andreae, M. O.; Warren, S. G. Oceanic Phytoplankton, Atmospheric Sulphur, Cloud Albedo and Climate. *Nature* **1987**, 326, 655–661.
- (2) Barnes, I.; Hjorth, J.; Mihalopoulos, N. Dimethyl Sulfide and Dimethyl Sulfoxide and Their Oxidation in the Atmosphere. *Chem. Rev.* **2006**, *106*, 940–975.
- (3) Hoffmann, E. H.; Tilgner, A.; Schrödner, R.; Bräuer, P.; Wolke, R.; Herrmann, H. An Advanced Modeling Study on the Impacts and Atmospheric Implications of Multiphase Dimethyl Sulfide Chemistry. *Proc. Natl. Acad. Sci. U.S.A.* **2016**, *113*, 11776–11781.
- (4) Rasmussen, F. R.; Kubetka, J.; Elm, J. Contribution of Methanesulfonic Acid to the Formation of Molecular Clusters in the Marine Atmosphere. *J. Phys. Chem. A* **2022**, *126*, 7127–7136.
- (5) Fung, K. M.; Heald, C. L.; Kroll, J. H.; Wang, S.; Jo, D. S.; Gettelman, A.; Lu, Z.; Liu, X.; Zaveri, R. A.; Apel, E. C.; et al. Exploring Dimethyl Sulfide (DMS) Oxidation and Implications for Global Aerosol Radiative Forcing. *Atmos. Chem. Phys.* **2022**, 22, 1549–1573.
- (6) Saltzman, E. S.; Savoie, D. L.; Zika, R. G.; Prospero, J. M. Methane Sulfonic Acid in the Marine Atmosphere. *J. Geophys. Res.: Oceans* **1983**, *88*, 10897–10902.
- (7) Hopkins, R. J.; Desyaterik, Y.; Tivanski, A. V.; Zaveri, R. A.; Berkowitz, C. M.; Tyliszczak, T.; Gilles, M. K.; Laskin, A. Chemical Speciation of Sulfur in Marine Cloud Droplets and Particles: Analysis of Individual Particles from the Marine Boundary Layer over the California Current J. Geophys. Res.: Atmos. 2008, 113, DOI: 10.1029/2007[D008954.
- (8) Sorooshian, A.; Padró, L. T.; Nenes, A.; Feingold, G.; McComiskey, A.; Hersey, S. P.; Gates, H.; Jonsson, H. H.; Miller, S. D.; Stephens et al. On the Link between Ocean Biota Emissions, Aerosol, and Maritime Clouds: Airborne, Ground, and Satellite Measurements off the Coast of California *Global Biogeochem*. *Cycles*2009, 23, DOI: 10.1029/2009GB003464.
- (9) Gaston, C. J.; Pratt, K. A.; Qin, X.; Prather, K. A. Real-Time Detection and Mixing State of Methanesulfonate in Single Particles at an Inland Urban Location during a Phytoplankton Bloom. *Environ. Sci. Technol.* **2010**, *44*, 1566–1572.
- (10) Eisele, F. L.; Tanner, D. J. Measurement of the Gas Phase Concentration of H_2SO_4 and Methane Sulfonic Acid and Estimates of H_2SO_4 Production and Loss in the Atmosphere. *J. Geophys. Res.: Atmos.* **1993**, *98*, 9001–9010.
- (11) Berresheim, H.; Elste, T.; Tremmel, H. G.; Allen, A. G.; Hansson, H.-C.; Rosman, K.; Dal Maso, M.; Mäkelä, J. M.; Kulmala, M.; O'Dowd, C. D. Gas-Aerosol Relationships of H₂SO₄, MSA, and OH: Observations in the Coastal Marine Boundary Layer at Mace Head, Ireland. *J. Geophys. Res.: Atmos.* **2002**, *107*, PAR5-1–PAR 5-12. (12) Bork, N.; Elm, J.; Olenius, T.; Vehkamäki, H. Methane Sulfonic Acid-Enhanced Formation of Molecular Clusters of Sulfuric Acid and

Dimethyl Amine. Atmos. Chem. Phys. 2014, 14, 12023-12030.

https://doi.org/10.1021/acs.jpca.3c01395 J. Phys. Chem. A XXXX, XXX, XXX—XXX

I

- (13) (a) Chen, H.; Ezell, M. J.; Arquero, K. D.; Varner, M. E.; Dawson, M. L.; Gerber, R. B.; Finlayson-Pitts, B. J. New Particle Formation and Growth from Methanesulfonic Acid, Trimethylamine and Water. *Phys. Chem. Chem. Phys.* **2015**, *17*, 13699–13709; (b) Chen, H.; Ezell, M. J.; et al. Correction: New particle formation and growth from methanesulfonic acid, trimethylamine and water. *Phys. Chem. Chem. Phys.* **2017**, *19*, 4893.
- (14) Dawson, M. L.; Varner, M. E.; Perraud, V.; Ezell, M. J.; Gerber, R. B.; Finlayson-Pitts, B. J. Simplified Mechanism for New Particle Formation from Methanesulfonic Acid, Amines, and Water via Experiments and Ab Initio Calculations. *Proc. Natl. Acad. Sci. U.S.A.* **2012**, *109*, 18719–18724.
- (15) Chen, H.; Varner, M. E.; Gerber, R. B.; Finlayson-Pitts, B. J. Reactions of Methanesulfonic Acid with Amines and Ammonia as a Source of New Particles in Air. *J. Phys. Chem. B* **2016**, *120*, 1526–1536.
- (16) Perraud, V.; Xu, J.; Gerber, R. B.; Finlayson-Pitts, B. J. Integrated Experimental and Theoretical Approach to Probe the Synergistic Effect of Ammonia in Methanesulfonic Acid Reactions with Small Alkylamines. *Environ. Sci. Process. Impacts* **2020**, 22, 305—328.
- (17) Chen, D.; Wang, W.; Li, D.; Wang, W. Atmospheric Implication of Synergy in Methanesulfonic Acid-Base Trimers: A Theoretical Investigation. *RSC Adv.* **2020**, *10*, 5173–5182.
- (18) Chackalackal, S. M.; Stafford, F. E. Infrared Spectra of Methane-, Fluoro-, and Chlorosulfonic Acids. *J. Am. Chem. Soc.* **1966**, 88, 4815–4819.
- (19) Durig, J. R.; Zhou, L.; Schwartz, T.; Gounev, T. Fourier Transform Raman Spectrum, Vibrational Assignment and Ab Initio Calculation of Methanesulfonic Acid in the Gas and Liquid Phases. *J. Raman Spectrosc.* **2000**, *31*, 193–202.
- (20) Zhong, L.; Parker, S. F. Structure and Vibrational Spectroscopy of Methanesulfonic Acid. R. Soc. Open Sci. 2018, 5, No. 181363.
- (21) Mihalopoulos, N.; Barnes, I.; Becker, K. H. Infrared Absorption Spectra and Integrated Band Intensities for Gaseous Methanesulphonic Acid (MSA). *Atmos. Environ., Part A* **1992**, *26*, 807–812.
- (22) Allen, H. C.; Raymond, E. A.; Richmond, G. L. Surface Structural Studies of Methanesulfonic Acid at Air /Aqueous Solution Interfaces Using Vibrational Sum Frequency Spectroscopy. *J. Phys. Chem. A* **2001**, *105*, 1649–1655.
- (23) Chen, X.; Allen, H. C. Water Structure at Aqueous Solution Surfaces of Atmospherically Relevant Dimethylsulfoxide and Methanesulfonic Acid by Phase-Sensitive Sum-Frequency Spectroscopy. *J. Phys. Chem. B* **2010**, *114*, 14983–14988.
- (24) Givan, A.; Loewenschuss, A.; Nielsen, C. J. Infrared Spectrum and Ab Initio Calculations of Matrix Isolated Methanesulfonic Acid Species and Its 1:1 Water Complex. *J. Mol. Struct.* **2005**, 748, 77–90.
- (25) Lane, J. R.; Kjaergaard, H. G.; Plath, K. L.; Vaida, V. Overtone Spectroscopy of Sulfonic Acid Derivatives. *J. Phys. Chem. A* **2007**, *111*, 5434–5440.
- (26) Huff, A. K.; Love, N.; Smith, C. J.; Leopold, K. R. Parent, ³⁴S, and Deuterated Triflic Acid: Microwave Spectra and Tunneling Splittings Due to Hydroxyl Torsion. *J. Mol. Spectrosc.* **2022**, 385, No. 111623.
- (27) Huff, A. K.; Love, N.; Leopold, K. R. Microwave Study of Triflic Acid Hydrates: Evidence for the Transition from Hydrogen-Bonded Clusters to a Microsolvated Ion Pair. *J. Phys. Chem. A* **2021**, 125, 8033–8046.
- (28) Love, N.; Huff, A. K.; Leopold, K. R. Proton Transfer in a Bare Superacid-Amine Complex: A Microwave and Computational Study of Trimethylammonium Triflate. *J. Phys. Chem. A* **2021**, *125*, 5061–5068.
- (29) Guthrie, J. P. Hydrolysis of Esters of Oxy Acids: pKa Values for Strong Acids; Brønsted Relationship for Attack of Water at Methyl; Free Energies of Hydrolysis of Esters of Oxyacids, and a Linear Relationship between Free Energy of Hydrolysis and pKa Holding Over a Range of 20 pK Units. Can. J. Chem. 1978, 56, 2342–2354.
- (30) Frisch, M. J.; Trucks, G. W.; Schlegel, H. B.; Scuseria, G. E.; Robb, M. A.; Cheeseman, J. R.; Scalmani, G.; Barone, V.; Petersson,

- G. A.; Nakatsuji, H.; Al, E.et al. Gaussian16; Gaussian, Inc.: Wallingford CT, 2016.
- (31) Wang, L. Clusters of Hydrated Methane Sulfonic Acid $CH_3SO_3H \cdot (H_2O)_n$ (n = 1-5): A Theoretical Study. *J. Phys. Chem. A* **2007**, 111, 3642–3651.
- (32) Krishtal, A.; Senet, P.; V Alsenoy, C. V. Influence of Structure on the Polarizability of Hydrated Methane Sulfonic Acid Clusters. *J. Chem. Theory Comput.* **2008**, *4*, 2122–2129.
- (33) Wen, H.; Huang, T.; Wang, C.-Y.; Peng, X.-Q.; Jiang, S.; Liu, Y.-R.; Huang, W. A Study on the Microscopic Mechanism of Methanesulfonic Acid-Promoted Binary Nucleation of Sulfuric Acid and Water. *Atmos. Environ.* **2018**, *191*, 214–226.
- (34) Chen, D.; Li, D.; Wang, C.; Luo, Y.; Liu, F.; Wang, W. Atmospheric Implications of Hydration on the Formation of Methanesulfonic Acid and Methylamine Clusters: A Theoretical Study. *Chemosphere* **2020**, 244, No. 125538.
- (35) Jørgensen, S.; Jensen, C.; Kjaergaard, H. G.; Anglada, J. M. The Gas-Phase Reaction of Methane Sulfonic Acid with the Hydroxyl Radical without and with Water Vapor. *Phys. Chem. Chem. Phys.* **2013**, *15*, 5140–5150.
- (36) Leopold, K. R. Hydrated Acid Clusters. *Annu. Rev. Phys. Chem.* **2011**, *62*, 327–349.
- (37) Phillips, J. A.; Canagaratna, M.; Goodfriend, H.; Grushow, A.; Almlöf, J.; Leopold, K. R. Microwave and Ab Initio Investigation of HF-BF₃. *J. Am. Chem. Soc.* **1995**, *117*, 12549–12556.
- (38) Dewberry, C. T.; Mackenzie, R. B.; Green, S.; Leopold, K. R. 3D-Printed Slit Nozzles for Fourier Transform Microwave Spectroscopy. *Rev. Sci. Instrum.* **2015**, *86*, No. 065107.
- (39) Canagaratna, M.; Phillips, J. A.; Goodfriend, H.; Leopold, K. R. Structure and Bonding of the Sulfamic Acid Zwitterion: Microwave Spectrum of ⁺H₃N-SO₃. *J. Am. Chem. Soc.* **1996**, *118*, 5290–5295.
- (40) Watson, J. K. G. Aspects of Quartic and Sextic Centrifugal Effects on Rotational Energy Levels. In *Vibrational Spectra and Structure*; Durig, J. R., Ed.; Elsevier: Amsterdam, 1977; pp 1–89.
- (41) Pickett, H. M. The Fitting and Prediction of Vibration-Rotation Spectra with Spin Interactions. *J. Mol. Spectrosc.* **1991**, *148*, 371–377.
- (42) Pickett, H. M. Vibration-Rotation Interactions and the Choice of Rotating Axes for Polyatomic Molecules. *J. Chem. Phys.* **1972**, *56*, 1715–1723.
- (43) Buschmann, P.; Lengsfeld, K. G.; Aydt, K.; Jahn, M. K.; Herbers, S.; Travers, M. J.; Nguyen, H. V. L.; Grabow, J.-U. Proton Inversion Tunneling in the Rotational Spectrum of Acetone Cyanohydrin. *J. Mol. Spectrosc.* **2020**, *373*, No. 111372.
- (44) Medel, R. Simple Models for the Quick Estimation of Ground State Hydrogen Tunneling Splittings in Alcohols and Other Compounds. *Phys. Chem. Chem. Phys.* **2021**, 23, 17591–17605.